Dual-Mode EPR Detects the Initial Intermediate in Photoassembly of the Photosystem II Mn Cluster: The Influence of Amino Acid Residue 170 of the D1 Polypeptide on Mn Coordination

Kristy A. Campbell,[§] Dee Ann Force,[‡] Peter J. Nixon,[||] François Dole,[⊥] Bruce A. Diner,*[,‡] and R. David Britt*[,§]

Contribution from the Department of Chemistry, University of California, Davis, California 95616, Experimental Station, E.I. duPont de Nemours Company, Wilmington, Delaware 19880-0173, Department of Biochemistry, Imperial College of Science, Technology and Medicine, London SW7 2AY, United Kingdom, and DRFMC/SCIB/3MC, CEA-Grenoble, 38054 Grenoble Cedex 9, France

Received January 11, 2000. Revised Manuscript Received February 23, 2000

Abstract: We report the first parallel polarization EPR signal from the Mn(III) ion formed by photooxidation of Mn(II) bound at the high affinity Mn-binding site of photosystem II (PSII). This species corresponds to the first photoactivation intermediate formed on the pathway to assembly of the water-splitting Mn cluster. The parallel mode EPR spectrum of the photooxidation product of 1.2/1 stoichiometry Mn(II)/Mn-depleted wild-type *Synechocystis* sp. PCC 6803 PSII particles consists of six well-resolved transitions split by a relatively small ^{55}Mn hyperfine coupling (44 G). This spectral signature is absent in photooxidized Mn apoPSII complexes prepared from D1-Asp170Glu and D1-Asp170His mutants, providing direct spectral evidence for a role for this specific D1-Asp170 residue in the initial photoactivation chemistry. Temperature-dependence measurements and spectral simulations performed on the Mn(III) parallel mode EPR signal of the wild-type sample give an axial zero-field splitting value of $D \approx -2.5$ cm^{-1} and a rhombic zero-field splitting value of $|E| \approx 0.269$ cm^{-1}. The negative D value for this d^4 ion is indicative of either a $^5B_{1g}$ symmetry ground state of an octahedral Mn(III) geometry or a $^5B_1$ symmetry ground state of a five-coordinate square-pyramidal Mn(III) geometry. The parallel mode Mn(III) EPR spectrum obtained from the wild-type photooxidized Mn apoPSII complex is contrasted with that obtained from the five-coordinate Mn(III) form of native Mn superoxide dismutase, which has a trigonal-bipyramidal geometry and a $^5A_1$ symmetry ground state giving rise to a positive D value and a much larger ^{55}Mn hyperfine coupling of 100 G. The D1-Asp170His mutant displays a parallel mode EPR spectrum similar to that observed in a Mn(III) model complex. The D1-Asp170Glu mutant shows no parallel mode spectrum, but in perpendicular mode it shows a broad feature near $g = 5$ which has spectral characteristics of an $S = {}^3/_2$ Mn(IV) ion. This suggests that this mutant provides a binding site with a less positive Mn(III)/Mn(IV) reduction potential.

Photosystem II of oxygenic photosynthesis utilizes a tetranuclear Mn cluster and a redox active tyrosine residue (Y_Z) to couple the reduction of the photooxidized Chl species P_{680}^+ to the enzymatic oxidation of water to dioxygen.[1] The same photochemistry is utilized to assemble the Mn cluster through a process termed "photoactivation",[2−6] where bioavailable Mn(II) ions are oxidized to the higher Mn(III)/Mn(IV) valencies of the catalytic cluster. The first photooxidation event occurs at a unique high-affinity Mn(II) binding site, where Mn(II) is oxidized to Mn(III) by the neutral $Y_Z^\bullet$ radical formed upon the coupled deprotonation and oxidation of Y_Z by P_{680}^+.[3] It is likely, but not yet rigorously proven, that this first photooxidation site remains a Mn ligation site for the intact Mn cluster. Mutagenesis studies have implicated the D1 protein residue aspartate-170 in high affinity binding of this photooxidizable Mn(II).[4]

There have been relatively few EPR investigations of photoactivation. Ananyev and Dismukes[5] have characterized a potential Mn(II)−Mn(II) dimer signal present when Mn(II) is added in the dark to apoPSII along with Ca^{2+}, but it has been suggested by others that this Mn(II)−Mn(II) dimer is not on the direct pathway to the tetranuclear Mn cluster.[3] A weak 6-line perpendicular mode $g = 8.3$ EPR signal, likely due to Mn(II) bound in a low-symmetry environment, is found in dark samples under low Ca^{2+} conditions.[5] This may be a signature of Mn(II) bound in the high-affinity site. No EPR observation of light-induced Mn(III) signals has been reported, despite the clear importance of directly observing the initial photooxidation intermediate. Indeed, the integer spin $S = 2$ Mn(III) ion is very difficult to observe with traditional perpendicular polarization

* To whom correspondence should be addressed. R.D.B.: Phone (530) 752-6377; Fax (530) 752-8995; E-mail rdbritt@ucdavis.edu. B.A.D.: Phone (302) 695-2494; Fax (302) 695-9183; E-mail Bruce.A.Diner@USA.dupont.com.

[§] University of California.

[‡] E.I. duPont de Nemours Company.

[||] Imperial College of Science, Technology and Medicine.

[⊥] DRFMC/SCIB/3MC.

(1) (a) Britt, R. D. Oxygen Evolution. In *Oxygenic Photosynthesis: The Light Reactions*; Ort, D. R., Yocum, C. F., Eds.; Kluwer Academic Publishers: Dordrecht, The Netherlands, 1996; pp 137−164. (b) Debus, R. J. *Biochim. Biophys. Acta* **1992**, *1102*, 269−352. (c) Yachandra, V. K.; Sauer, K.; Klein, M. P. *Chem. Rev.* **1996**, *96*, 2927−2950.

(2) Tamura, N.; Cheniae, G. M. *Biochim. Biophys. Acta* **1987**, *890*, 179−194.

(3) Ono, T.; Mino, H. *Biochemistry* **1999**, *38*, 8778−8785.

(4) Nixon, P. J.; Diner, B. A. *Biochemistry* **1992**, *31*, 942−948.

(5) Ananyev, G. M.; Dismukes, G. C. *Biochemistry* **1997**, *36*, 11342−11350.

10.1021/ja000142t CCC: $19.00
Published on Web 03/30/2000

EPR spectroscopy at X-band or comparable frequencies,[7] thus giving rise to the lore that Mn(III) is an EPR-silent species. However, we have previously employed X-band parallel polarization EPR spectroscopy to characterize the $S = 2$ Mn(III) ion of oxidized Mn superoxide dismutase (MnSOD),[8] demonstrating that highly hyperfine-resolved Mn EPR spectra can be obtained for Mn(III) bound at enzymatic sites using this alternate excitation geometry. In this report, we extend the use of parallel polarization EPR to detect the spectroscopic signature of the Mn(III) ion formed by the photooxidation of Mn(II) bound at the high-affinity site of PSII. This species corresponds to the first photoactivation intermediate (designated L_1 by Tamura and Cheniae[2]) formed on the pathway to assembly of the water-splitting Mn cluster of photosystem II. In addition, both parallel and perpendicular mode EPR is used to examine the photooxidation products of the D1-D170 mutants.

Materials and Methods

Biochemical Preparations. Site-directed mutations D1-Asp170Glu (D1-D170E) and D1-Asp170His (D1-D170H) were constructed in *Synechocystis* PCC. 6803 by Nixon and Diner.[4] A hexahistidine tag was introduced at the C-terminus of the PSII protein CP47 in the D1-D170E mutant and in the phycocyanin-deficient ("Olive") wild-type strains, and the corresponding PSII core complexes were isolated by Ni(II)-affinity chromatography.[9] PSII core complexes from the D1-D170H mutant were isolated as described by Tang and Diner.[10] "Apo"-PSII core particles were prepared by Mn-depleting PSII core complexes with a 5 mM hydroxylamine treatment for 30 min on ice,[11] followed by the addition of 1 mM EDTA and passage through a desalting column (Econopac 10-DG, Biorad) equilibrated with Buffer A (MES−NaOH (pH 6.1), 20 mM $CaCl_2$, 5 mM $MgCl_2$, 25% glycerol (w/v), and 0.03% (w/v) dodecyl maltoside). The apoPSII complexes were then concentrated using a Centricon YM-100 (Millipore). Each sample was made 300 μM in both K_3FeCN_6 and PPBQ, and a 1.2-fold excess of Mn(II) vs reaction center (assuming 38 Chl per reaction center[10]) was added as the chloride salt (wild-type sample: apoPSII concentration, 0.130 mM and $MnCl_2$, 0.156 mM; both mutant samples: apoPSII concentration, 0.122 mM and $MnCl_2$, 0.146 mM). The Mn apoPSII core complexes were loaded into EPR tubes and deoxygenated by purging with argon. Finally, photooxidized Mn apoPSII complexes were trapped by freezing under illumination (5000 W/m^2) for 30 s. Following EPR characterization, optical characterization of the wild-type and mutant samples was performed after removing the Mn by EDTA treatment. An aliquot of the EPR sample was treated with a concentration of EDTA 3.3-fold that of the Mn and then washed with Buffer A on a Centricon YM-100. The final concentration of EDTA in the sample used for optical measurements was <50 nM.

EPR Spectroscopy. Continuous-wave EPR spectra were recorded on a Bruker ECS106 X-band CW-EPR system with a Bruker ER 4116DM dual mode cavity capable of both parallel (TE012) and perpendicular (TE102) mode polarizations of the applied magnetic field. Cryogenic temperatures were obtained with an Oxford ESR900 liquid helium cryostat. The temperature was controlled with an Oxford ITC503 temperature and gas flow controller.

Simulation Methodology. An $S = 2$ CW-EPR spectral simulation program was written[12] that includes a Boltzmann distribution to account for temperature dependence, a transition probability calculation for both parallel and perpendicular orientation of the applied oscillating magnetic field, a Gaussian line shape function, and orientation variation of the molecular crystal axes with respect to the static magnetic field to account for the randomly oriented molecules within a frozen glass sample.

The Hamiltonian used to simulate the CW-EPR spectrum of the Mn-(III) wild-type species generated in PSII is:

$$\hat{H} = \beta_e \vec{B}_0 \cdot \tilde{g}_e \cdot \hat{S} + D\left[\hat{S}_z^2 - \frac{1}{3}S(S+1)\right] + E(\hat{S}_x^2 - \hat{S}_y^2) + \hat{S} \cdot \tilde{A} \cdot \hat{I} \quad (1)$$

The terms, from left to right, are the electron Zeeman, the axial zero-field splitting, the rhombic zero-field splitting, and the electron−nuclear hyperfine interactions. In this equation, β_e is the electron Bohr magneton, $\vec{B}_0$ is the applied static magnetic field, $\tilde{g}_e$ is the electron g tensor, $\hat{S}$ is the net electron spin operator, $\tilde{A}$ is the hyperfine tensor, D is the axial zero-field splitting value, E is the rhombic zero-field splitting value, $\hat{I}$ is the nuclear spin operator for the Mn ($I = {}^5/_2$) nucleus, and S is the total electron spin magnitude ($S = 2$ for a high-spin Mn(III) ion). The principal molecular axis is defined as the z-axis for the zero-field splitting tensor, $\tilde{D}$, where the axial zero-field splitting value D is ${}^3/_2 D_{zz}$. The static magnetic field, $\vec{B}_0$, is considered to be oriented arbitrarily to the principal molecular axis within the first octant of the sphere describing the molecular geometry (θ, ϕ orientation). The transition-inducing oscillating magnetic field ($\vec{B}_1$) is along $\vec{B}_0$ for parallel polarization EPR simulations. θ and ϕ are both evenly varied from 0 to 90°, with the solid angle weighting performed by multiplying the transition probability by $\sin\theta\, d\theta\, d\phi$. EPR line shapes are achieved by use of a Gaussian line shape function. For these simulations, the zero-field splitting tensor and g-tensor axes are assumed to be collinear with the principal molecular axis.

Results

The D1-D170E strain grows photosynthetically while the D1-D170H strain is only weakly photoautotrophic. Both show oxygen evolution rates that are reduced compared to wild-type (D1-D170E, 60−100% of wild-type; D1-D170H, 20−40% of wild-type), and both have relatively high affinity for the photooxidizable Mn(II) as determined by the titration of the blockage by Mn(II) of charge recombination between the reduced acceptor quinone Q_A^- and the PSII donor side.[4] The K_M value for photooxidizable Mn(II) binding for wild-type is 1.5 ± 0.5 μM (90%), as compared to 3 ± 0.4 μM (88%) for D1-D170E and 10 ± 3.6 μM (82%) for D1-D170H,[13] where the listed percentages correspond to the percentage of the total kinetic fit represented by the listed K_M value for Mn(II) binding. These results are similar to previously reported results (ref 4). Each K_M value reflects a combination of the binding affinity of Mn(II) in the dark to the site at which it can reduce $Y_Z^\bullet$ and the rate at which it diffuses to this site during the lifetime of the charge-separated state following a flash of light. In both cases the ability to block charge recombination is linearly proportional to the Mn(II) concentration at concentrations less than K_M. Given the greater than 100 μM concentrations of Mn(II) added in 1.2-fold excess to the apoPSII cores, the high-affinity Mn(II)

(6) Zaltsman, L.; Ananyev, G. M.; Bruntrager, E.; Dismukes, G. C. *Biochemistry* **1997**, *36*, 8914−8922.

(7) (a) For an example of EPR observation of Mn(III) in rutile see: Gerritsen, H. J.; Sabisky, E. S. *Phys. Rev.* **1963**, *132*, 1507−1512. (b) In addition, a parallel polarization study of synthetic Mn(III) complexes has been previously performed (Dexheimer, S. L.; Gohdes, J. W.; Chan, M. K.; Hagen, K. S.; Armstrong, W. H.; Klein, M. P. *J. Am. Chem. Soc.* **1989**, *111*, 8923−8925); however, this study showed at best poor resolution of ^{55}Mn hyperfine features.

(8) Campbell, K. A.; Yikilmaz, E.; Grant, C. V.; Gregor, W.; Miller, A. F.; Britt, R. D. *J. Am. Chem. Soc.* **1999**, *121*, 4714−4715.

(9) Reifler, M. J.; Chisholm, D. A.; Wang, J.; Diner, B. A.; Brudvig, G. W. Engineering and Rapid Purification of Histidine-tagged Photosystem II from *Synechocystis* PCC 6803. In *Photosynthesis: Mechanisms and Effects*; Garab, G., Ed.; Kluwer Academic Publishers: Dordrecht, The Netherlands, 1998; pp 1189−1192.

(10) Tang, X.-S.; Diner, B. A. *Biochemistry* **1994**, *33*, 4594−4603.

(11) Tamura, N.; Cheniae, G. M. *Biochim. Biophys. Acta* **1985**, *809*, 245−259.

(12) LS Fortran software for the Power Macintosh; Fortner Research LLC: Sterling, VA 20164, 1996.

(13) The mutant PSII values quoted here are from measurements taken in parallel with the EPR spectra on the indentical samples, and are slightly higher than the 2 μM for D1-D170E and 2−10 μM for D1-D170H values reported previously.[4]

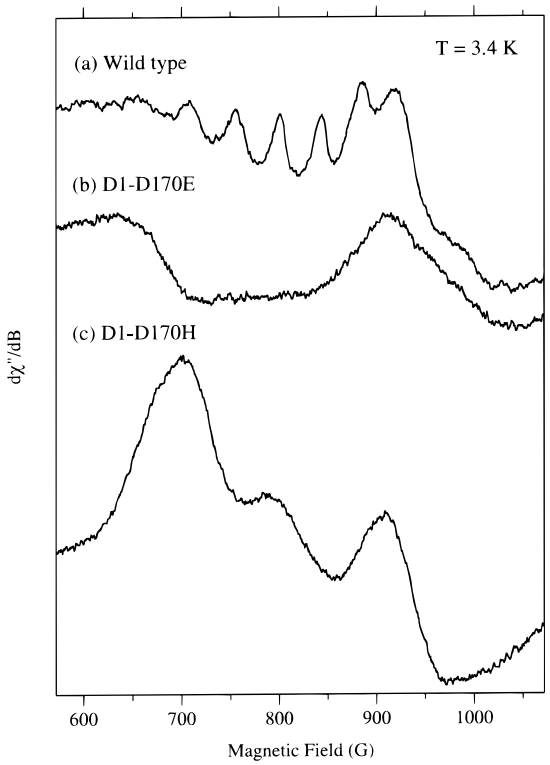

Figure 1. Parallel mode CW-EPR spectra obtained at a temperature of 3.4 K. Trace a reveals the Mn(III) spectrum of the photooxidized Mn apoPSII wild-type *Synechocystis* complex. Traces b (D1-D170E mutant) and c (D1-D170H mutant) display the PSII mutant spectra obtained under identical conditions as for the wild-type sample in trace a. Experimental conditions are as follows: microwave frequency, 9.409 GHz; microwave power, 25 mW; modulation amplitude, 8 G; modulation frequency, 100 kHz; time constant, 163.84 ms; conversion time, 81.92 ms.

oxidation site should be 90−100% occupied for both mutants as well as for wild-type.[14]

Figure 1 shows the parallel polarization X-band CW-EPR spectra of the photooxidized Mn apoPSII (a) wild-type, (b) D1-D170E, and (c) D1-D170H complexes, each recorded at a temperature of 3.4 K. In the wild-type sample (a), a six-line EPR spectrum is observed at an effective g value of approximately 8.2, with a hyperfine splitting of ≈44 G. No comparable signal is observed in the perpendicular polarization mode. Given the spectral similarity of the wild-type spectrum to the Mn(III) SOD spectrum[8] and also to several synthetic Mn(III) complexes,[15] we assign the signal to photooxidized Mn(III), specifically the first photoassembly intermediate L_1.

Under identical EPR spectral acquisition conditions, the six-line Mn(III) signal is totally absent in the photooxidized Mn apoPSII complexes prepared from the D1-D170E (Figure 1b) and D1-D170H (Figure 1c) mutants. Each of these mutants is capable of Mn(II) photooxidation,[4] and therefore the photooxidized Mn apoPSII complexes contain Mn(III) (or Mn(IV), *vide infra*), but are not coordinated in a fashion that gives rise to a hyperfine-resolved parallel polarization EPR spectrum.

(14) The 20% excess of added Mn(II) does not contribute to hyperfine-resolved parallel mode features, either as Mn(II) or as oxidized Mn(III), as determined by the lack of such features in the mutant samples. Also, we note that wild-type spectra obtained in samples isolated by the Tang et al. procedure[10] show the same Mn(III) six-line spectrum, indicating that this is not an artifact of the histidine tag isolation method.

(15) Campbell, K. A. CW and Pulsed EPR Studies of Photosystem II and Mn-Containing Complexes, Ph.D. Dissertation, University of California, Davis, 1999.

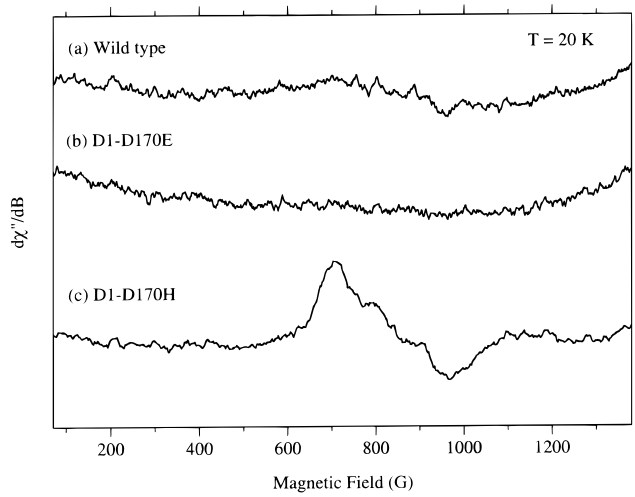

Figure 2. Parallel mode CW-EPR spectra obtained at a temperature of 20 K: (a) wild-type; (b) D1-D170E; and (c) D1-D170H. Experimental parameters are the same as in Figure 1 except the temperature.

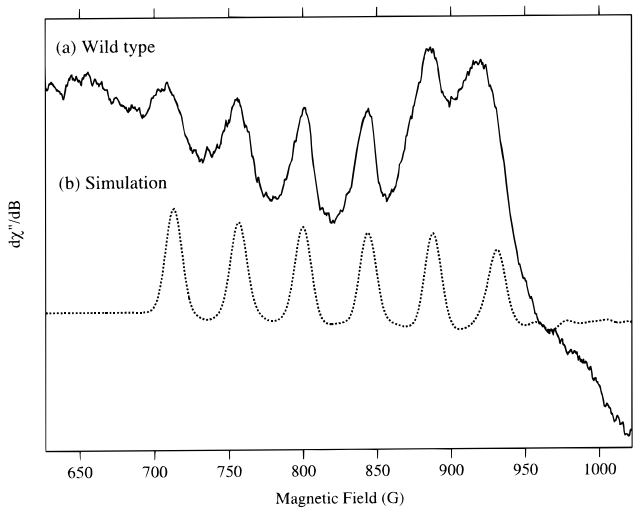

Figure 3. (a) Parallel mode CW-EPR signal of the wild-type sample and (b) the spectral simulation. Simulation parameters are $D = -2.5$ cm^{-1}; $E = 0.269$ cm^{-1}; $g_\perp = 2.00$; $g_\parallel = 1.98$; $|A_\perp| = 68$ G; $|A_\parallel| = 44$ G. Additionally, in the spectral simulation, θ was incremented from 0.1° to 89.7° evenly using 448 steps of 0.2° each. ϕ was incremented evenly from 0.1° to 88.1° using 11 steps of 8° each. The transition probability was weighted by sin θ as described in the text. The line shape width is 5 G.

At higher temperatures (20 K), the wild-type and the D1-D170E samples show no detectable parallel mode EPR signals (Figure 2a,b). However, at the higher temperature, a parallel polarization EPR signal is observed in the D1-D170H sample (Figure 2c). This EPR signal is centered at an effective g value of approximately 8.2, the same g value as the six-line signal observed in the wild-type, but it does not show any clearly resolved hyperfine structure. The signal seen at 20 K is also observed at 3.4 K (Figure 1c). At 20 K its amplitude is reduced by a factor of 2.5.

A simulation of the wild-type Mn(III) spectrum is displayed in Figure 3 along with the experimental data. Simulation parameters are as follows: axial zero-field splitting, $D = -2.5$ cm^{-1}; rhombic zero-field splitting, $E = 0.269$ cm^{-1}; $g_\perp = 2.00$; $g_\parallel = 1.98$; $A_\perp = 68$ G; $A_\parallel = 44$ G; and line shape width, 5 G. Varying the $A_\perp$ hyperfine parameters has little effect on the simulation, the expected result given that the observed six-line EPR signal corresponds to the parallel turning point of the

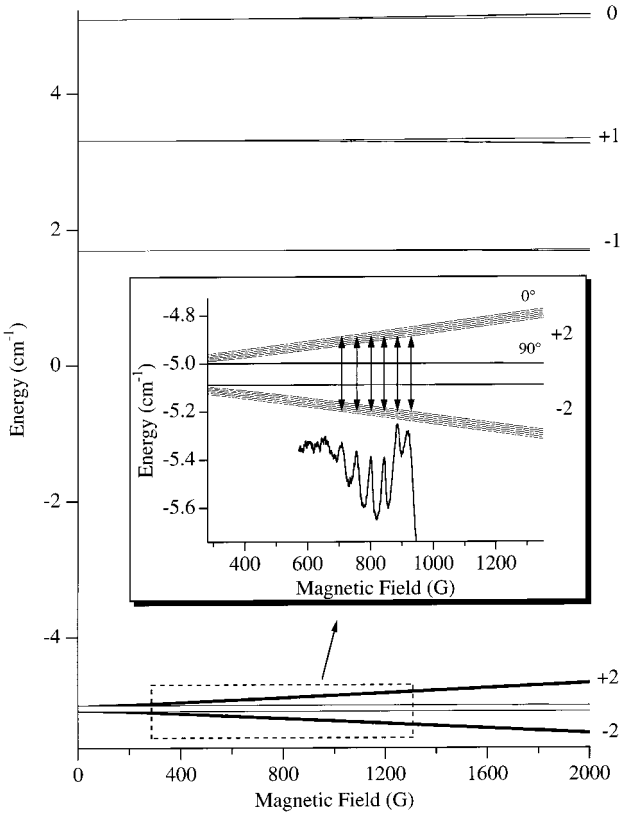

Figure 4. Energy level diagram for an $S = 2$ spin system constructed using the simulation parameters listed in the caption of Figure 3. The energy levels for $\theta = 0$ and 90° ($\phi = 0°$) are displayed. Inset: The observed EPR transitions occur between the $M_s = \pm 2$ levels (high-field notation) for $\theta \approx 0°$.

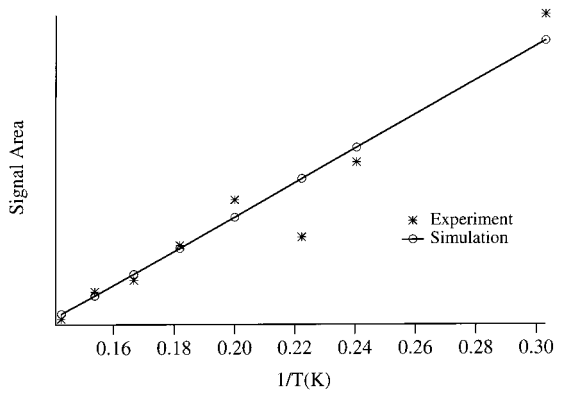

Figure 5. Temperature dependence of the wild-type EPR signal area vs $1/T$ and a simulated temperature dependence. The simulated temperature dependence parameters are the same as those used to obtain the spectral simulation shown in Figure 3.

overall EPR powder pattern.[8] This is illustrated in the energy level diagram shown in Figure 4.

The temperature dependence of the wild-type six-line hyperfine-resolved Mn(III) spectrum, plotted in Figure 5 as signal area vs $1/T$, exhibits Curie law ($\propto 1/T$) behavior. This Curie law behavior, with signal intensity decreasing with increasing temperature, is indicative of a negative axial zero-field splitting value, D, where the $M_s = \pm 2$ manifolds (high-field notation) giving rise to the EPR signal lie lowest in energy (see Figures 4 and 9). The temperature-dependence data were collected at a nonsaturating microwave power (25 mW) over the temperature range of 3.3 to 7 K. At 7 K the detectable signal is quite small, and it is virtually undetectable at 9 K (data not shown). The

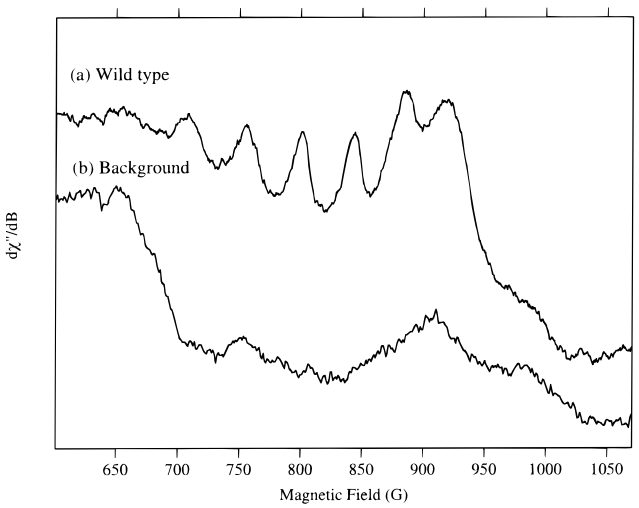

Figure 6. Parallel mode CW-EPR spectra of (a) the wild-type photooxidized Mn apoPSII sample (from Figure 1) compared to (b) the background signal normally present in PSII samples. The background spectrum was collected from an oxygen-evolving wild-type *Synechocystis* sample in the dark-adapted S_1 state. The experimental conditions are the same as in Figure 1. Note: The S_1 state multiline signal is not observable in this figure since it occurs at a lower magnetic field than shown.

temperature-dependence data are well simulated (solid line) with the same parameters used in the spectral simulation (Figure 3b). The temperature dependence simulation procedure is the same as described previously.[8]

Underlying the six-line EPR spectrum is a background signal frequently observed in samples in the parallel mode, and especially troublesome when looking at samples with small concentrations such as these dilute photosystem II samples (maximum [Mn(III)] = 130 μM). An example of this background signal is shown in Figure 6b, in this case from an oxygen-evolving wild-type *Synechocystis* sample in its resting state (S_1 state). A comparison with the photogenerated Mn(III) wild-type EPR signal, Figure 6a, shows that the background signal distorts the intensities of the hyperfine lines relative to each other and partially obscures the highest field hyperfine feature. This background feature thus hinders a quantitative comparison of the simulated signal intensity with that of the experimental data. It should be noted that the magnetic field range shown for the background signal in Figure 6b is outside the field range of S_1 state multiline signal also present in this sample.

Returning to the mutant samples, the $T = 3.4$ K D1-D170E EPR spectrum (Figure 1b) is quite similar to the background spectrum (Figure 6b), indicating a lack of a parallel mode Mn(III) signal in the D1-D170E mutant. However, the D1-D170H mutant shows another parallel mode EPR spectrum (Figures 1c and 2c) that is quite different from the background spectrum. That the D1-D170H parallel mode spectrum could also be arising from a Mn(III) ion is apparent when the spectrum of the D1-D170H mutant obtained at 20 K is compared with the parallel mode spectrum of Mn(III)salen[16] (Figure 7). We are currently working to more fully describe the detailed line shape and temperature dependence of the Mn(III)salen complex,[17] for

(16) Mn(III)salen, (*R*,*R*)-(−)-*N*,*N*-bis(3,5-di-*tert*-butylsalicylidene)-1,2-cyclohexanediamino manganese(III) chloride.

(17) The temperature dependence of the parallel mode EPR signal of the Mn(III)salen complex prepared in dry CH_2Cl_2 solvent is quite complex, with at least two additional sets of six hyperfine lines each with different temperature dependence (Campbell, K. A.; Wyatt, J. K.; Nantz, M. H.; Britt, R. D. Manuscript in preparation).

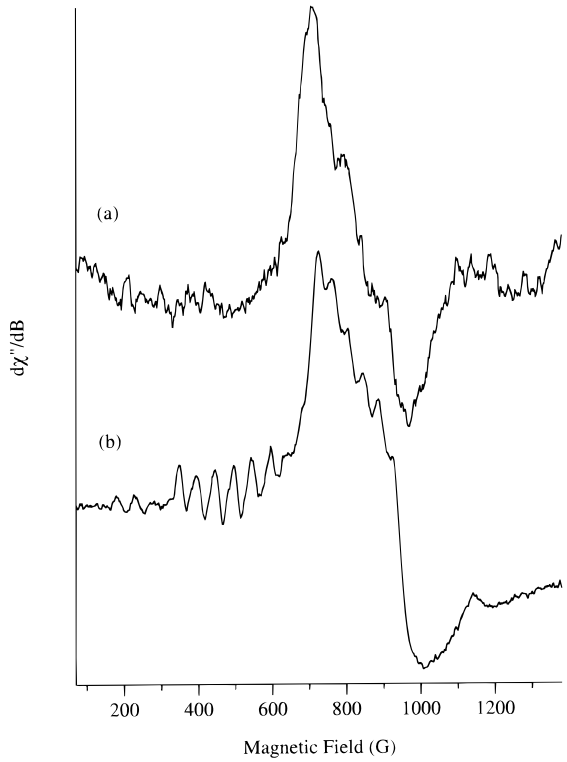

Figure 7. Parallel mode CW-EPR spectra of (a) D1-D170H mutant, collected at 20 K (from Figure 2c) compared to (b) Mn(III)salen in CH_2Cl_2 collected at 4.1 K. Experimental conditions for part a are given in Figure 2. Experimental conditions for part b are as follows: microwave frequency, 9.409 GHz; microwave power, 1 mW; modulation amplitude, 10 G; modulation frequency, 100 kHz; time constant, 20.48 ms; conversion time, 40.96 ms.

example, to understand why its spectrum differs from the simple six-line spectrum often observed.[15] We show this spectrum to note the remarkable similarity to the D1-D170H spectrum.

Not only is a Mn(III) parallel mode signal absent from the D1-D170E mutant spectrum, but there is only a small $g = 2$ perpendicular mode Mn(II) EPR signal indicating that much of the Mn(II) was photooxidized. Inspection of the low-field perpendicular mode EPR spectrum shows the presence of a peak at an effective g value of approximately 5.7 (Figure 8a). This peak is remarkably similar to the EPR spectra of Mn(IV) ions of Mn model complexes.[15] Figure 8 shows the D1-D170E perpendicular mode EPR spectrum compared with the Mn(IV) perpendicular mode EPR spectra from Mn(salen) in (b) a mixture of Mn(III) and Mn(IV) oxidation states and (c) purely the Mn(IV) state (preparation details in Figure 8 caption). The $g = 5.7$ feature in the D1-D170E mutant closely matches the Mn(IV) feature in the Mn(III)/Mn(IV)salen mixture, while the Mn(IV) feature in the Mn(IV)salen monomer spectrum is shifted to a slightly lower g value ($g = 5.4$). The $g = 8$ hyperfine-containing feature in the Mn(III)/Mn(IV)salen mixture is from the Mn(III) form. As with the Mn(III)salen parallel mode case, experiments to further characterize the perpendicular mode spectral features of Mn(IV)salen are in progress, and these preliminary spectra are presented to support the assignment of Mn(IV) generated in the D1-D170E mutant.[17]

Discussion

Magnetic Properties of the Wild-Type Mn(III). As discussed in our previous work,[8] due to large axial zero-field splitting values for typical $S = 2$ Mn(III) ions (D ranging from -1 to -4 cm^{-1} for mononuclear Schiff-base complexes and

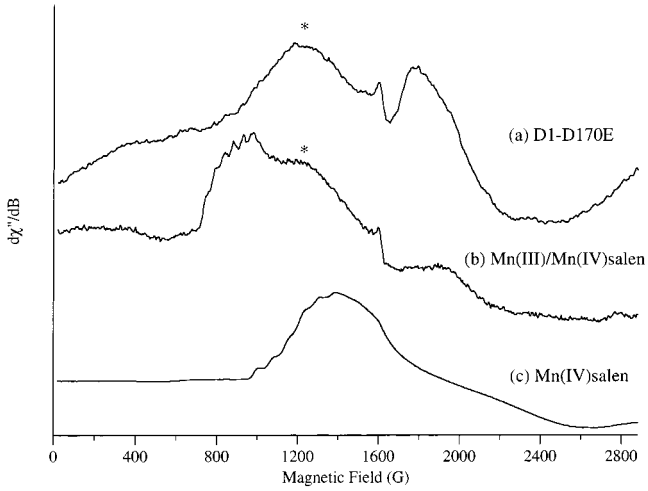

Figure 8. Perpendicular mode EPR spectra of (a) D1-D170E mutant; (b) Mn(III)/Mn(IV)salen mixture; and (c) Mn(IV)salen. The peaks marked by asterisks in parts a and b are at an effective g value of 5.7. An overlay of these features shows that they align exactly. The hyperfine-containing peak at $g = 8$ in part b is due to Mn(III)salen. Experimental conditions are as follows: microwave frequency, 9.67 GHz; microwave power, 3 (a) and 1 (b and c) mW; modulation amplitude, 10 G; modulation frequency, 100 kHz; time constant, 40.96 ms; conversion time, 81.92 ms. The Mn(III)/Mn(IV)salen mixture was generated by an addition of 65 μL of a 0.38 M solution of *m*-chloroperbenzoic acid in CH_2Cl_2 to the top surface of a 110 μL frozen (77 K) solution of Mn(III)salen (5 mM) and *N*-methylmorpholine *N*-oxide (10 mM) in an EPR tube, then allowing the sample to warm to 195 K for 30 s. The Mn(IV)salen species in part c was generated by allowing the mixture from part b to incubate at 195 K for 5 min.

-1 to -3 cm^{-1} for Mn(III) porphyrins[18]), the conventional perpendicular polarization EPR-allowed $\Delta M_s = \pm 1$ transitions have much smaller transition probabilities at X-band microwave frequencies than the corresponding parallel polarization EPR case where transitions occur between the closely spaced $M_s = \pm 2$ energy levels (often referred to as a non-Kramers doublet[19]), or they are not observable since the $\Delta M_s = \pm 1$ levels may be split by more than $h\nu$. In addition to the disadvantage of a lower transition probability amplitude obtained with perpendicular polarization, biological samples typically show adventitious perpendicular mode EPR signals in the low-field region which would likely obscure the observation of any small Mn(III) perpendicular mode signal.[20] These considerations make parallel polarization EPR ideally suited to the observation of integer spin EPR signals such as that from Mn(III) in PSII or MnSOD.

The Mn(III) parallel mode EPR spectrum observed in the wild-type photooxidized PSII sample almost certainly arises from a high-spin $S = 2$ complex with a ^{5}D electronic ground term. A priori, the molecular geometry of the Mn(III) center is unknown. The limiting geometries of the likely candidates include a five-coordinate site with square-pyramidal (SP; C_{4v} point group) or trigonal-bipyramidal (TBP; D_{3h} point group) geometry or a six-coordinate site with octahedral geometry (O_h

(18) (a) Kennedy, B. J.; Murray, K. S. *Inorg. Chem.* **1985**, *24*, 1557−1560. (b) Behere, D. V.; Mitra, S. *Inorg. Chem.* **1980**, *19*, 992−995. (c) Goldberg, D. P.; Tesler, J.; Krzystek, J.; Montalban, A. G.; Brunel, L.-C.; Barrett, A. G. M.; Hoffman, B. M. *J. Am. Chem. Soc.* **1997**, *119*, 8722−8723. (d) Kennedy, B. J.; Murray, K. S. *Inorg. Chem.* **1985**, *24*, 1552−1557.

(19) Abragam, A.; Bleaney, B. *Electron Paramagnetic Resonance of Transition Ions*; Oxford University Press: London, 1970; Chapter 15.

(20) (a) Miller, A.-F.; Brudvig, G. W. *Biochim. Biophys. Acta* **1991**, *1056*, 1−18. (b) Peterson, J.; Fee, J. A.; Day, E. P. *Biochim. Biophys. Acta* **1991**, *1079*, 161−168.

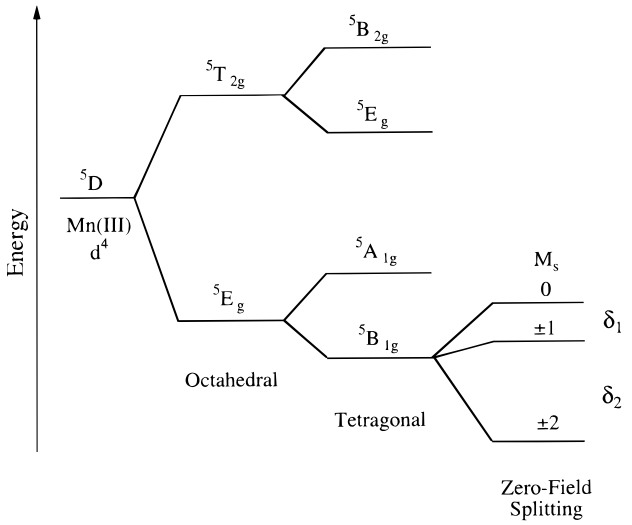

Figure 9. State splitting diagram showing the effects of Jahn−Teller distortion and spin−orbit coupling on the $S = 2$, ^{5}D term with initial octahedral symmetry at zero magnetic field. The octahedral symmetry is split into a tetragonal field. The three M_s levels shown at zero-field are labeled using the high-field notation. The case shown is for a negative zero-field splitting, D. The splitting between the M_s levels designated δ_1 and δ_2 is D and 3D, respectively (where D is the axial zero-field splitting value), in the absence of any hyperfine or rhombic zero-field splitting interactions ($A = 0$; $E = 0$).

point group). In an octahedral field, the ^{5}D term will split into $^5T_{2g}$ and ^5E_g terms (Figure 9). The 2-fold degeneracy of the ^5E_g ground state will be removed by spin−orbit coupling and Jahn−Teller distortions, yielding a tetragonal field with either a $^5A_{1g}$ or $^5B_{1g}$ ground state term (Figure 9). The terms shown in the tetragonal field in Figure 9 are also those that are found in the five-coordinate SP geometry (excluding the gerade notation). Ultimately it is the symmetry of the ligand field about the Mn(III) ion that determines the ground-state term. A $^5A_{1g}$ ground state, in which the $d_{x^2-y^2}$ orbital is occupied and the d_{z^2} orbital is unoccupied, results in a compression of the d_{z^2} orbital. In this case the zero-field splitting, D, will be positive due to second-order effects of the spin−orbit coupling energy.[21] This case occurs for both the TBP ($^5A_1$ ground state)[22] and tetragonally compressed octahedral geometries. A ground state $^5B_{1g}$ term, in which the d_{z^2} orbital is occupied and the $d_{x^2-y^2}$ orbital is unoccupied, results in an elongation of the d_{z^2} orbital. In this case, the zero-field splitting value, D, is negative. This case occurs for both the SP ($^5B_1$ ground state) and tetragonally elongated octahedral geometries. Given the negative D value (-2.5 cm^{-1}) obtained from the temperature dependence and simulations of the Mn(III) photoassembly intermediate experimental data (Figure 5), the geometry could be either six-coordinate tetragonally elongated or five-coordinate square pyramidal.

The Mn(III) site in native MnSOD (which also gives rise to a six-line parallel mode EPR spectrum[8]) is observed in the crystal structure to be five-coordinate in a roughly TBP geometry.[23] For MnSOD, the axial zero-field splitting value, D, obtained from the temperature dependence and spectral

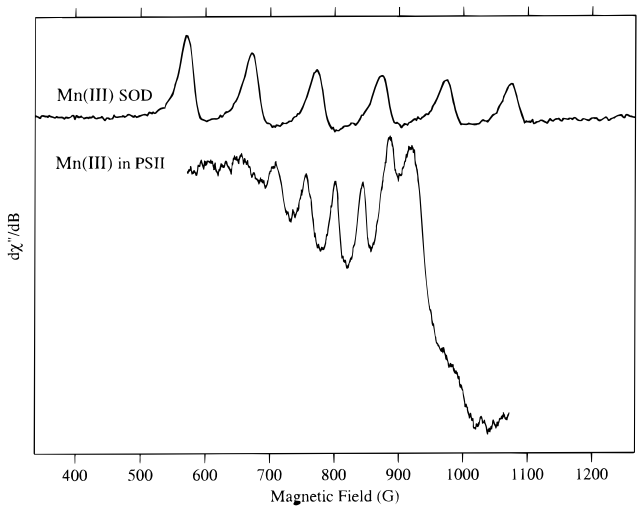

Figure 10. Parallel mode CW-EPR spectra of Mn(III)SOD (from ref 8) and the PSII *Synechocystis* wild-type Mn(III) photoassembly intermediate. The MnSOD hyperfine spacing is approximately 100 G, whereas the PSII Mn(III) hyperfine spacing is approximately 44 G.

simulations of the parallel mode EPR spectrum is positive (+2.1 cm^{-1}), as expected for a $^5A_1$ TBP geometry.[22] The resolved hyperfine spacing in the MnSOD spectrum is ∼100 G (parallel hyperfine value, $|A_{||}| = 100$ G). In contrast (Figure 10), the Mn(III) photooxidation PSII species gives rise to a parallel mode signal with hyperfine spacing of only ∼44 G ($|A_{||}| = 44$ G). The difference between the magnitude of the $A_{||}$ values between the positive D (MnSOD) and negative D (Mn(III) photoactivation PSII intermediate) cases is predicted from the equations for the parallel and perpendicular hyperfine values that take into account the effects of spin−orbit coupling:[7a,21a,24]

$$|A_{||}| = \left|P\left(\pm\frac{1}{7} - \kappa + g_{||} - 2\right)\right| \quad (2)$$

$$|A_{\perp}| = \left|P\left(\mp\frac{1}{14} - \kappa + g_{\perp} - 2\right)\right| \quad (3)$$

where $g_{||} = 2 - (4 \pm 4)\lambda/\Delta$, $g_{\perp} = 2 - (4 \mp 2)\lambda/\Delta$ (with λ = spin−orbit coupling constant and Δ = doublet/triplet splitting), $P = 2\beta_e\beta_N g_N \langle r^{-3}\rangle$ (where r is the electron−nuclear distance and g_N is 1.3819 for ^{55}Mn), and κ is a dimensionless constant arising from an additional isotropic hyperfine interaction due to mixing of the d orbitals with excited electron configurations containing unpaired s electrons.[21a,24] The coefficient κ has been experimentally determined to be almost identical for all iron group ions (such as Mn(III), Ti(III), and Cr(II)).[24] In eqs 2 and 3, the top sign is selected for the tetragonally elongated octahedral or SP geometries ($^5B_{1g}$ or $^5B_1$ ground state, respectively; i.e., the Mn(III) PSII case) and the bottom sign is selected for the tetragonally compressed octahedral ($^5A_{1g}$ ground state) and TBP ($^5A_1$ ground state; MnSOD) cases.

These equations yield $|A_{||}|$ and $|A_{\perp}|$ values for the PSII Mn(III) intermediate:

$$|A_{||}| = \left|P\left(+\frac{1}{7} - \kappa - \frac{8\lambda}{\Delta}\right)\right| \quad (4)$$

$$|A_{\perp}| = \left|P\left(-\frac{1}{14} - \kappa - \frac{2\lambda}{\Delta}\right)\right| \quad (5)$$

(21) (a) Griffith, J. S. *The Theory of Transition-Metal Ions*; Cambridge University Press: London, 1971. (b) See also the derivation shown in: Krzystek, J.; Telser, J.; Pardi, L. A.; Goldberg, D. P.; Hoffman, B. M.; Brunel, L.-C. *Inorg. Chem.* **1999**, *38*, 6121−6129.

(22) Whittaker, J. W.; Whittaker, M. M. *J. Am. Chem. Soc.* **1991**, *113*, 5528−5540.

(23) Ludwig, M. L.; Metzger, A. L.; Pattridge, K. A.; Stallings, W. C. *J. Mol. Biol.* **1991**, *219*, 335−358.

whereas for MnSOD, $|A_{||}|$ and $|A_{\perp}|$ values are given by:

$$|A_{||}| = \left|P\left(-\frac{1}{7} - \kappa\right)\right| \quad (6)$$

$$|A_{\perp}| = \left|P\left(+\frac{1}{14} - \kappa - \frac{6\lambda}{\Delta}\right)\right| \quad (7)$$

A direct comparison of eqs 4 and 6 shows that for similar P (same order of magnitude), λ/Δ small, and similar κ values (e.g. $\kappa = 0.5$)[7a] in the Mn(III) PSII and MnSOD cases, $|A_{||}|_{PSII}$ will be less than $|A_{||}|_{MnSOD}$. This is indeed what is observed.

In addition, with the reasonable assumption that κ is similar for the two types of samples,[24] a comparison can be made between the dipolar and isotropic hyperfine coupling constants expected for the two cases. A_{dip} and A_{iso} can be expressed in terms of $A_{||}$ and $A_{\perp}$:[25]

$$A_{dip} = \frac{A_{||} - A_{\perp}}{3} \quad (8)$$

$$A_{iso} = \frac{A_{||} + 2A_{\perp}}{3} \quad (9)$$

Thus, for the case of the Mn(III) PSII EPR signal, A_{iso} and A_{dip} are:

$$A_{dip} = P\left(\frac{1}{14} - \frac{2\lambda}{\Delta}\right) \quad (10)$$

$$A_{iso} = P\left(-\kappa - \frac{4\lambda}{\Delta}\right) \quad (11)$$

and for the MnSOD Mn(III) EPR signal, A_{iso} and A_{dip} are:

$$A_{dip} = P\left(-\frac{1}{14} + \frac{2\lambda}{\Delta}\right) \quad (12)$$

$$A_{iso} = P\left(-\kappa - \frac{4\lambda}{\Delta}\right) \quad (13)$$

A comparison of A_{dip} in the two different cases (eqs 10 and 12) shows that A_{dip} is identical except for a change in sign, whereas A_{iso} is the same. However, this direct comparison is somewhat shortsighted in that it assumes that P is identical for the two different samples.

Using $\kappa = 0.5$,[7a] $\lambda/\Delta = 2.5 \times 10^{-3}$, and the measured value $|A_{||}| \approx 44$ G for the PSII Mn(III) intermediate, P can be calculated from eq 4 to be $|P| = 111 \times 10^{-4}$ cm^{-1}. This yields a projected value of $|A_{\perp}| = 68$ G (we again note that $A_{\perp}$ is not resolved in the parallel mode experiment). In addition, with $\lambda/\Delta = 2.5 \times 10^{-3}$, the resulting g tensor values are $g_{||} = 1.98$ and $g_{\perp} = 2.00$. These values agree well with the simulations (see Table 1 and Figures 3 and 5). A similar calculation can be performed for the MnSOD sample. Assuming the same values of κ and λ/Δ yields $|P| = 145 \times 10^{-4}$ cm^{-1} (Equation 6), consequentially giving $|A_{\perp}| = 69$ G. Additionally, for the MnSOD case, calculations yield $g_{||} = 2.0$ and $g_{\perp} = 1.99$. These values also agree with experimental data (Table 1).

The dipolar and isotropic hyperfine coupling constants can be calculated from eqs 10 through 13 using the same assumptions as above. These calculated values are given in Table 1.

Table 1. Summary of Experimental and Calculated Results for the $^5B_{1g}$ and $^5A_1$ Ground States[a]

	$^5B_{1g}$ or $^5B_1$	$^5A_1$
$\|A_{||}\|$[b]	44.8 G	100 G
$\|A_{\perp}\|$	68.5 G	69 G
$\|P\|$[c]	111×10^{-4} cm^{-1}	145×10^{-4} cm^{-1}
$g_{||}$	1.98	2.00
$g_{\perp}$	2.00	1.99
A_{dip}	$\pm$7.9 G	$\mp$10.3 G
A_{iso}	$\mp$60.6 G	$\mp$79.2 G

[a] All values shown are calculated from eqs 4−13, unless otherwise indicated. The calculations assume $\kappa = 0.5$ and $\lambda/\Delta = 2.5 \times 10^{-3}$. [b] These values are measured from the parallel mode CW-EPR spectra. [c] $P = 2\beta_e\beta_N g_N\langle r^{-3}\rangle$.

Notice that for the PSII Mn(III) intermediate ($^5B_{1g}$ or $^5B_1$ ground state), A_{dip} and A_{iso} are necessarily of different signs. Conversely, the MnSOD Mn(III) center ($^5A_1$ ground state) gives values of A_{dip} and A_{iso} of the same sign.

The hyperfine and zero-field splitting parameters derived from this study show that the first photoactivation intermediate is in an environment similar to a six-coordinate tetragonally-elongated or a five-coordinate square-pyramidal geometry. Back-calculations[26] of Mn(III) hyperfine parameters from Mn(III,IV) dimer model complexes give hyperfine values of $A_{||} = 50$ to 70 G and $A_{\perp} = 78$ to 85 G.[27] However, Mn(III) model complexes yield $A_{||}$ values of 38 to 60 G.[7,15,17a,b] The $A_{||}$ values from the Mn(III) model complexes bracket the 44 G value of the Mn(III) photoactivation intermediate. None of the Mn(III) hyperfine values back-calculated from Mn(III,IV) dimer model complexes or measured from Mn(III) model complexes yield hyperfine values as large as $A_{||}$ for the MnSOD sample. In addition, the axial zero-field splitting values for the typical Mn(III) model complexes are negative. Thus, given the relationship between the sign of D and the magnitude of $A_{||}$, the results for the MnSOD are consistent with the anticipated trigonal-bipyramidal geometry, distinct from the values derived from Mn(III,IV) dimers and Mn(III) model complexes investigated to date, including the PSII photoactivation intermediate described here.

Biological Significance. The electron transfer kinetics experiments on PSII complexes isolated from wild-type and a series of mutants have provided support for D1-aspartate170 playing a direct role in the binding of the high-affinity photooxidizable Mn(II), perhaps as a direct ligand. Our parallel polarization EPR results, which show a dramatic alteration of magnetic and redox properties of the photooxidized Mn ion in these mutants, provides strong additional evidence for D1-aspartate 170 ligation of this first photooxidized intermediate in Mn cluster formation. Interestingly, the D1-D170H mutant shows what is most likely an altered form of a Mn(III) parallel mode EPR spectrum, as evidenced by a comparison between its EPR spectrum at 20 K and that from Mn(III)salen. The D1-D170E mutant shows evidence for a Mn(IV) species (Figure 8) or possibly a weakly coupled Mn(IV,IV) dimer[15] in the perpendicular mode EPR

(24) Al'tshuler, S. A.; Kozyrev, B. M. *Electron Paramagnetic Resonance in Compounds of Transition Elements*; John Wiley & Sons: New York, 1974.

(25) Weltner, W., Jr. *Magnetic Atoms and Molecules*; Dover Publications: New York, 1983; p 204.

(26) In Mn(III,IV) dimers, the observed $A_{||}$ values range from −396 to 297 MHz for Mn(III) and +235 to +204 MHz for Mn(IV); however, because of the antiferromagnetic exchange coupling between the Mn(III) and Mn(IV) in the dimer, the observed hyperfine values differ from the intrinsic values by factors of +2 and −1 (referred to as projection factors) for the Mn(III) and Mn(IV) ions, respectively. For a full discussion, see: Randall, D. W.; Chan, M. K.; Armstrong, W. H.; Britt, R. D. *Mol. Phys.* **1998**, *95*, 1283−1294.

(27) (a) Cooper, S. R.; Dismukes, G. C.; Klein, M. P.; Calvin, M. *J. Am. Chem. Soc.* **1978**, *100*, 7248−7252. (b) Zheng, M.; Khangulov, S. V.; Dismukes, G. C.; Barynin, V. V. *Inorg. Chem.* **1994**, *33*, 382−387. (c) Goodson, P. A.; Hodgson, D. J.; Glerup, J.; Michelsen, K.; Weihe, H. *Inorg. Chem.* **1991**, *30*, 4909−4914. (d) Lubitz, W.; Zweygart, W.; Bittl, R.; Wieghardt, K.; Haselhorst, G.; Weyhermüller, T. In *Bioinorganic Chemistry*; Trautwein, A. X., Ed.; VCH Publishers: Berlin, 1997.

spectrum, and no evidence of Mn(III) in the parallel mode. These results indicate that the D1-D170E mutant is capable of oxidizing the tightly bound Mn(II) species all the way to Mn(IV); however, as evidenced by the EPR spectra, the PSII centers in the wild-type and D1-D170H mutant are capable of generating only the Mn(III) state. Further study is required to understand how the D1-D170 ligand exerts redox control over the bound high-affinity Mn ion.

Conclusions

Parallel polarization EPR allows detection of the initial Mn(III) photoactivation intermediate of wild-type PSII. This ^{55}Mn hyperfine-resolved Mn(III) center joins that of MnSOD and a number of Mn(III) model complexes in showing well-resolved six-line parallel mode spectra. The spectral and temperature dependences of these signals allow characterization of the electronic ground states of these Mn(III) ions through the signs and magnitudes of the axial zero-field splitting parameter, D, and the magnitudes of the parallel hyperfine component $A_{||}$. A different class of Mn(III) parallel mode spectrum is observed in the D1-D170H mutant, and EPR characterization of the D1-D170E mutant supports photooxidation to the Mn(IV) state. The control extended by the D1-D170 ligand over magnetic and redox properties of the high-affinity Mn site provides strong support for its actual Mn ligation.

Acknowledgment. Support was provided by NIH (GM48242) to R.D.B. and by NRICGP/USDA (97-35306-4882) to B.A.D. MnSOD samples were kindly provided by Dr. Anne-Frances Miller and Emine Yikilmaz, University of Kentucky, Lexington. Also, we would like to thank Jamie Wang and Dexter Chisholm for engineering the His-tagged CP47 in the D1-D170E mutant strain.

JA000142T